Preclinical Evaluation and Quantification of ^{18}F-Fluoroethyl and ^{18}F-Fluoropropyl Analogs of SCH442416 as Radioligands for PET Imaging of the Adenosine A_{2A} Receptor in Rat Brain

Shivashankar Khanapur[1], Aren van Waarde[1], Rudi A.J.O. Dierckx[1], Philip H. Elsinga[1], and Michel J.B. Koole[1,2]

[1]*Department of Nuclear Medicine and Molecular Imaging, University of Groningen, University Medical Center Groningen, Groningen, The Netherlands; and* [2]*Department of Nuclear Medicine and Molecular Imaging, KU Leuven, Leuven, Belgium*

The cerebral adenosine A_{2A} receptor is an attractive therapeutic target for neuropsychiatric disorders. ^{18}F-fluoroethyl and ^{18}F-fluoropropyl analogs of ^{18}F-labeled pyrazolo[4,3-e]-1,2,4-triazolo [1,5-c]pyrimidine (SCH442416) (^{18}F-FESCH and ^{18}F-FPSCH, respectively) were developed as A_{2A} receptor–specific PET ligands. Our aim was to determine an appropriate compartmental model for tracer kinetics, evaluate a reference tissue approach, and select the most suitable PET ligand. **Methods:** A 90-min dynamic PET scan with arterial blood sampling and metabolite analysis was acquired for 22 healthy male Wistar rats starting at the time of ^{18}F-FESCH ($n = 12$) and ^{18}F-FPSCH ($n = 10$) injection. For each tracer, half the animals were vehicle-treated whereas the other half were pretreated with the A_{2A} receptor–selective antagonist KW-6002, inducing full blocking. Regional tissue total volume of distribution (V_T) was estimated by 1- and 2-tissue-compartment modeling (1TCM and 2TCM, respectively) and Logan graphical analysis. Midbrain, cerebellum, and hippocampus were evaluated as the reference region by comparing baseline V_T with V_T under full blocking conditions and comparing striatal nondisplaceable binding potential (BP_{ND}) using a simplified reference tissue model (SRTM) with distribution volume ratio minus 1 (DVR − 1) for 60- and 90-min scans. **Results:** On the basis of the Akaike information criterion, 1TCM and 2TCM were the most appropriate models for ^{18}F-FPSCH (baseline striatal V_T, 3.7 ± 1.1) and ^{18}F-FESCH (baseline striatal V_T, 5.0 ± 2.0), respectively. Baseline striatal V_T did not significantly differ between tracers. After pretreatment, striatal V_T was reduced significantly, with no significant decrease in hippocampus, midbrain, or cerebellum V_T. Baseline striatal SRTM BP_{ND} did not differ significantly from DVR − 1 except for ^{18}F-FPSCH when using a 60-min scan and midbrain as the reference region, whereas Bland–Altman analysis found a smaller bias for ^{18}F-FESCH and a 60-min scan. After pretreatment, striatal SRTM BP_{ND} did not significantly differ from zero except for ^{18}F-FPSCH when using hippocampus as the reference region. Striatal SRTM BP_{ND} using midbrain or cerebellum as the reference region was significantly lower for ^{18}F-FPSCH (range, 1.41–2.62) than for ^{18}F-FESCH (range, 1.64–3.36). **Conclusion:** Dynamic PET imaging under baseline and blocking conditions determined ^{18}F-FESCH to be the most suitable PET ligand for quantifying A_{2A} receptor expression in the rat brain. Accurate quantification is achieved by a 60-min dynamic PET scan and the use of either cerebellum or midbrain as the reference region.

Key Words: preclinical positron emission tomography (μPET); cerebral adenosine A_{2A} receptor; ^{18}F-SCH442416 analogs; kinetic analysis; rat brain

J Nucl Med 2017; 58:466–472
DOI: 10.2967/jnumed.116.178103

Adenosine, an extracellular endogenous signaling molecule, is released to either reduce the energy demand or increase the energy supply to a damaged or stressed organ or tissue and thereby elicits cytoprotective and neuromodulatory effects via 4 different G-protein–coupled adenosine receptors: A_1, A_{2A}, A_{2B}, and A_3 (*1–5*). Of these receptors, high-affinity A_1 and A_{2A} have been extensively studied because they are well characterized both pharmacologically and biochemically (*6*). The A_1 receptor is ubiquitously present within the human brain but has high expression levels in the hippocampus, cerebral cortex, thalamic nuclei, and dorsal horn of the spinal cord. The A_{2A} receptor is restricted to the basal ganglia and is particularly abundant in the striatum. Lower levels of A_{2A} receptor are expressed in several brain regions, including the hippocampus, cerebral cortex, amygdala, cerebellum, brain stem, and hypothalamus (*7–10*).

Many studies have reported a dysregulation of A_{2A} receptor in neuropsychiatric disorders such as Parkinson, Huntington, and Alzheimer diseases; attention deficit hyperactivity and panic disorders; schizophrenia; pain; and impaired sleep (*11*). Several studies have suggested that the A_{2A} receptor may play an important role in the regulation of dopaminergic and glutamatergic neurotransmission in the basal ganglia through antagonistic interactions with the dopamine D_2 receptor and by forming functional heterodimers with metabotropic glutamate receptor 5, cannabinoid receptor type 1, and the adenosine A_1 receptor (*12–14*). PET can be used with high-affinity and selective A_{2A} receptor antagonist radioligands to exploit changes in A_{2A} receptor distribution and density during disease progression and to monitor the response of such changes to treatment. Furthermore, PET can be used to assess A_{2A} receptor occupancy by investigational drugs in the human brain, thereby providing a useful tool for the drug discovery process (*11*).

Several PET radiotracers have been developed and evaluated for in vivo imaging of the A_{2A} receptor in the brain (*15–23*). We have developed ^{18}F-fluoroethyl and ^{18}F-fluoropropyl analogs of ^{18}F-labeled pyrazolo[4,3-e]-1,2,4-triazolo[1,5-c]pyrimidine (SCH442416) (^{18}F-FESCH and ^{18}F-FPSCH, respectively) (Fig. 1) and evaluated them in healthy rats (*6*). Preliminary evaluation of these tracers

Received May 11, 2016; revision accepted Oct. 2, 2016.
For correspondence or reprints contact: Michel Koole, Division of Nuclear Medicine, KU Leuven, Herestraat 49, 3000 Leuven, Belgium.
E-mail: michel.koole@kuleuven.be
Published online Oct. 27, 2016.

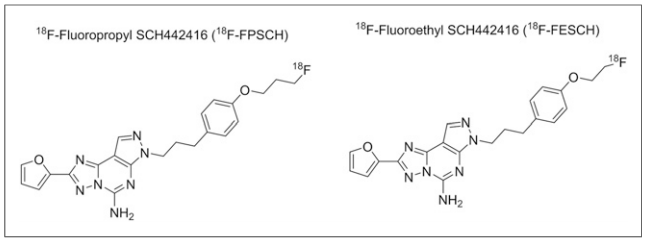

FIGURE 1. Chemical structures of ^{18}F-labeled SCH442416 analogs.

showed a distribution corresponding to the known regional A_{2A} receptor densities in rat brain. Moreover, both tracers demonstrated slightly different but reversible kinetics with a decreased nonspecific binding and an increased striatum-to-cerebellum ratio compared with ^{11}C-labeled pyrazolo[4,3-e]-1,2,4-triazolo[1,5-c]pyrimidine (^{11}C-SCH442416). Metabolite analyses indicated the presence of hydrophilic radiometabolites, which are not expected to cross the blood–brain barrier (*6*).

The aim of the present study was to develop a suitable tracer kinetic model for the quantification of the cerebral A_{2A} receptor with these radiofluorinated A_{2A} receptor ligands, to evaluate a reference tissue approach, and to determine whether there is a reduction in acquisition time.

MATERIALS AND METHODS

General

The compounds SCH442416 and KW-6002 were purchased from Axon Medchem BV, and 1,2-ethanediol di-p-tosylate and 1,3-propanediol di-p-tosylate were acquired from Sigma-Aldrich. All other chemicals were of analytic grade; were obtained from commercial suppliers such as Fluka, Rathburn, Sigma, and Merck; and were used without further purification.

Radiosynthesis of ^{18}F-FESCH and ^{18}F-FPSCH

The synthesis, radiolabeling, and quality control of ^{18}F-FESCH and ^{18}F-FPSCH were described in detail previously (*24*). In brief, tracers were prepared by a 2-step 2-pot radiosynthetic method, starting with the corresponding intermediate ^{18}F-fluorosynthons (2-^{18}F-fluoroethyltosylate and 3-^{18}F-fluoropropyltosylate), followed by selective fluoroalkylation of the *O*-desmethyl precursor.

Small-Animal PET Scanning

The animal experiments were performed by licensed investigators in compliance with the law on animal experiments of The Netherlands. The institutional animal care and use committee of the University of Groningen approved the protocols. Twenty-two male outbred Wistar-Unilever rats were included in the study design, subdivided into a control group and pretreated group for each tracer (Table 1). Five minutes before intravenous tracer administration, the pretreated animals were administered a cold A_{2A} receptor antagonist, KW-6002 (1 mg/kg, 50% dimethyacetamide:saline [v/v]), by intraperitoneal injection to prove saturability and specific binding of the tracers in the brain (*18,25*). Because the median effective dose of KW-6002 in rat striatum for intraperitoneal injection is 0.044–0.062 mg/kg, as demonstrated by a dose occupancy study with ^{11}C-preladenant, administration of a 1 mg/kg dose of KW-6002 by intraperitoneal injection is expected to fully block the A_{2A} receptor in rat brain (*23*). The volume of the vehicle (solvent) was 1 mL/kg, corresponding to a volume of 0.3 mL for an average rat with a weight of 300 g. For each animal, a dynamic PET scan was acquired and reconstructed with time frames of 8×30, 3×60, 2×120, 2×180, 3×300, 5×600, 1×480, and 1×960 s. The PET data were corrected for random coincidences, scatter, and attenuation. During the scan, blood samples were drawn at 0, 5, 10, 15, 20, 30, 45, 60, 75, and 90 s and 2, 3, 5, 7, 10, 15, 30, 60, and 90 min after injection. Plasma samples taken at intervals of 2, 5, 10, 15, 30, 60, and 90 min were applied for metabolite analysis using thin-layer chromatography to determine average population-based metabolite curves separately for the control and pretreated animals.

Male outbred Wistar-Unilever rats were obtained from Harlan. The animals were housed in Macrolon (Covestro) polycarbonate breeding cages ($38 \times 26 \times 24$ cm), maintained on a 12-h-light/12-h-dark regime, and fed standard laboratory chow (RMH-B) and water ad libitum. After arrival, the rats were allowed to acclimatize for at least 7 d. During PET imaging, all animals were anesthetized with isoflurane/medical air (inhalation anesthesia, 5% during induction, $\leq$2% during maintenance) and were kept on electronic heating pads during the entire study period. A femoral artery and a femoral vein were cannulated for blood sampling and tracer injection, respectively. A Harvard-style syringe pump at a speed of 1 mL/min was used for tracer injection. In addition, oxygen saturation and heart rate were measured using a pulse oximeter (Nonin) with an optical sensor attached to the hind leg. These parameters were maintained within physiologic limits by manual adjustment of the anesthesia parameters (isoflurane concentration and gas flow). In each scan session, 2 rats were scanned simultaneously (supine position) using a Focus 220 microPET camera (CTI, Siemens). The brains of both rats were placed in the field of view. Before the emission scan, a transmission scan of 515 s was obtained using a ^{57}Co point source. The emission scan was acquired in list mode for 106 min, starting at the moment the tracer entered the body of the first rat; the second animal was injected 16 min later. Dynamic PET data were acquired in list mode and rebinned into time frames of 8×30, 3×60, 2×120, 2×180, 3×300, 5×600, 1×480, and 1×960 s, with the first rebinning starting at the injection time of the first animal and the second rebinning taking into account the delayed injection of the second animal. Time frames were reconstructed using a 2-dimensional ordered-subsets expectation-maximization algorithm (4 iterations, 16 subsets, and zoom factor of 2). The reconstructed images were smoothed with a 3-dimensional gaussian filter (1.35 mm in full width at half maximum in both directions) and split so that a separate dataset was available for each animal with the

TABLE 1
Body Weight and Injected Dose

Parameter	^{18}F-FPSCH		^{18}F-FESCH	
	Control (n = 6)	Pretreated (n = 6)	Control (n = 5)	Pretreated (n = 5)
Body weight (g)	295 ± 19	293 ± 31	312 ± 14	321 ± 15
Injected mass dose (nM)	0.21 ± 0.11	0.29 ± 0.27	1.13 ± 0.41	0.74 ± 0.62

Pretreatment was done with KW-6002 (A_{2A} receptor antagonist, 1 mg/kg). Data are mean ± SD.

proper timings. During the dynamic PET scan, blood samples (0.1–0.15 mL) were taken from the cannulation of the femoral artery. After collecting 25 μL of whole blood, plasma (25 μL) was acquired from the remainder of the blood samples by short centrifugation (5 min at 1,000*g*). Radioactivity in both 25 μL of plasma and 25 μL of whole blood was counted on a γ-counter (CompuGamma 1282 CS; LKB-Wallac).

Small-Animal PET Data Analysis

Time–activity curves for the striatum, midbrain, cerebellum, and hippocampus were extracted from the dynamic PET data. Kinetic analysis was performed by fitting a 1TCM and a 2TCM to the time–activity curves using a blood- and metabolite-corrected plasma input function. Population average values were used as the input function in 2 pretreated ^{18}F-FPSCH animals for which arterial blood sampling was not available. Besides the compartment models, a Logan graphical analysis of the PET data was performed, with the linear fit starting at 9 min after injection. For both ^{18}F-FPSCH and ^{18}F-FESCH, distribution volume, V_T, was determined for 1TCM and 2TCM and Logan graphical analysis, and 1TCM and 2TCM fittings were compared using the Akaike information criterion.

PET data were analyzed using Inveon Research Workplace (Siemens Medical Solutions). The summed PET time frames from each animal were coregistered to an MRI template of a rat brain with predefined volumes of interest. Translation, rotation, and scaling were adjusted to visually optimize fusion of the images. Volumes of interest were transferred from the MRI template to the PET data, and tissue time–activity curves were extracted and rescaled to SUVs using measured body weight and injected dose. Compartmental models were fitted to the time–activity curves using blood- and metabolite-corrected data from arterial plasma samples and uncorrected data from whole-blood samples as input functions, with the fractional cerebral blood volume fixed to 3.6% (*1*). A single exponential was fitted to the parent fraction data, whereas a triple exponential was fitted to the whole blood and plasma radioactivity data. PET frames were weighted according to the frame duration and frame mid time relative to the start of the acquisition. A delay parameter describing a timing offset between tissue and blood data was fitted simultaneously with the compartment model.

Once the most appropriate compartmental model was determined, hippocampus, midbrain, and cerebellum were evaluated as reference regions by calculating the striatal distribution volume ratio minus 1 (DVR − 1) relative to each of these regions. Because blocking was expected to be complete for the pretreated animals, the DVR − 1 was not expected to differ significantly from 1. For the control group, striatal DVR − 1 was compared with nondisplaceable binding potential (BP_{ND}) using an SRTM for both a complete dynamic scan of 90 min and a dynamic scan of 60 min to assess the feasibility of reducing the acquisition time. We excluded cortical areas and brain regions close to the striatum as candidate reference regions, because such regions suffer from spillover effects from striatum-specific binding and from nonspecific tracer uptake in the Harderian glands or the skull because of possible tracer defluorination.

RESULTS

^{18}F-FPSCH and ^{18}F-FESCH V_T

1TCM, 2TCM, and Logan graphical analysis V_T data for ^{18}F-FPSCH and ^{18}F-FESCH in control and pretreated animals are presented in Table 2. The corresponding Akaike information criterion for 1TCM and 2TCM together with representative fits of both tracers is presented in Figure 2. For ^{18}F-FPSCH, the 2TCM Akaike information criterion proved to be lower than the 1TCM Akaike information criterion in 11 of 48 cases, suggesting that 1TCM is the most suitable model for ^{18}F-FPSCH. However, for ^{18}F-FESCH, the 2TCM Akaike information criterion was lower than the corresponding one for 1TCM in 35 of 40 cases, suggesting that 2TCM is the most appropriate compartmental model for ^{18}F-FESCH.

^{18}F-FPSCH. For ^{18}F-FPSCH V_T, 2-way repeated-measures ANOVA showed a significant interaction between brain region and model, with Bonferroni posttests revealing significant differences in average striatal V_T between 1TCM and the Logan plot but no significant difference between average 1TCM and 2TCM V_T in any brain region.

Because 1TCM is the preferred compartmental model to describe ^{18}F-FPSCH tracer kinetics, 1TCM V_T was further analyzed using 2-way repeated-measures ANOVA to determine the regional effect of pretreatment. This analysis showed a significant interaction between brain region and pretreatment, whereas Bonferroni posttests demonstrated a significant difference in average V_T between control and pretreated animals for the striatum but not for hippocampus, midbrain, or cerebellum.

For the pretreated animals, the 1TCM DVR − 1 representing striatal ^{18}F-FPSCH uptake relative to the hippocampus, midbrain, and cerebellum was, respectively, 1.10 ± 0.09, 1.04 ± 0.15, and 1.04 ± 0.11. In no case were these values significantly different from 1 (Wilcoxon signed rank test, $P > 0.05$).

TABLE 2
V_T for Striatum, Hippocampus, Midbrain, and Cerebellum Using 1TCM, 2TCM, and Logan Graphical Analysis

		^{18}F-FPSCH			^{18}F-FESCH		
Region	Group	1TCM	2TCM	Logan	1TCM	2TCM	Logan
STR	Control	3.69 ± 1.11 (30.00%)	3.72 ± 1.10 (29.53%)	3.52 ± 1.11 (31.62%)	4.80 ± 1.69 (35.21%)	5.00 ± 1.96 (39.13%)	4.66 ± 1.95 (41.96%)
	Pretreated	0.98 ± 0.38 (38.14%)	1.00 ± 0.39 (38.70%)	0.96 ± 0.32 (33.46%)	1.00 ± 0.28 (28.18%)	1.22 ± 0.26 (21.71%)	1.19 ± 0.20 (17.03%)
HC	Control	1.13 ± 0.29 (25.54%)	1.14 ± 0.32 (27.92%)	1.13 ± 0.26 (22.89%)	1.16 ± 0.21 (18.40%)	1.29 ± 0.29 (22.72%)	1.25 ± 0.30 (24.20%)
	Pretreated	0.90 ± 0.35 (39.41%)	0.91 ± 0.37 (40.73%)	0.98 ± 0.35 (35.37%)	0.75 ± 0.19 (25.03%)	1.10 ± 0.28 (25.56%)	1.00 ± 0.20 (19.66%)
MB	Control	1.16 ± 0.27 (22.96%)	1.17 ± 0.26 (22.34%)	1.15 ± 0.23 (20.39%)	1.15 ± 0.29 (25.13%)	1.26 ± 0.40 (31.43%)	1.22 ± 0.37 (30.26%)
	Pretreated	0.97 ± 0.39 (40.16%)	0.99 ± 0.40 (40.44%)	1.07 ± 0.49 (45.45%)	0.83 ± 0.15 (17.78%)	1.18 ± 0.41 (34.63%)	1.05 ± 0.15 (14.63%)
CB	Control	1.15 ± 0.29 (25.63%)	1.14 ± 0.29 (25.31%)	1.07 ± 0.29 (26.69%)	1.14 ± 0.27 (23.79%)	1.25 ± 0.34 (27.50%)	1.22 ± 0.35 (28.67%)
	Pretreated	0.95 ± 0.37 (38.85%)	0.97 ± 0.39 (39.90%)	0.96 ± 0.32 (33.44%)	0.82 ± 0.13 (15.62%)	1.40 ± 0.49 (35.11%)	1.14 ± 0.13 (11.47%)

CB = cerebellum; HC = hippocampus; MB = midbrain; STR = striatum.
Data are mean ± SD, followed by coefficient of variation in parentheses.

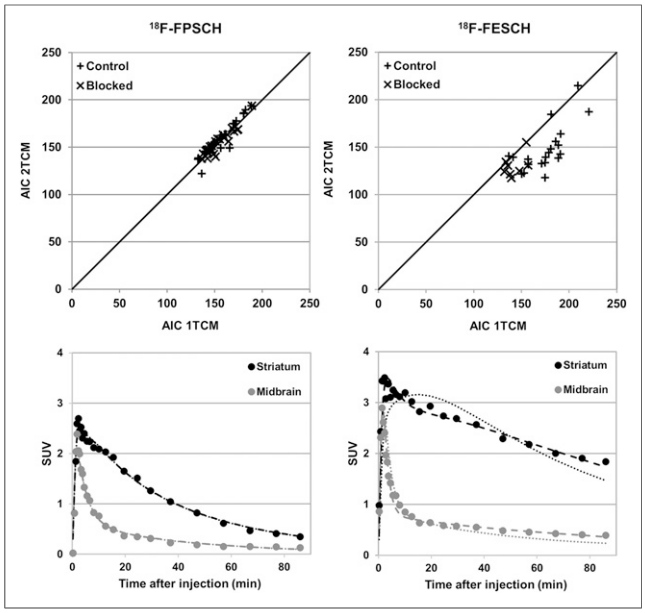

FIGURE 2. Akaike information criterion (AIC) for 1TCM and 2TCM (top) and representative 1TCM (dotted line) and 2TCM (dashed line) fitting (bottom) for ^{18}F-FPSCH and ^{18}F-FESCH.

^{18}F-FESCH. ^{18}F-FESCH V_T was analyzed using 2-way repeated-measures ANOVA. This analysis showed a significant interaction between brain region and model, with Bonferroni posttests revealing a significant difference in average V_T between 1TCM and 2TCM for the hippocampus and cerebellum but no significant difference between average Logan and 2TCM V_T in any brain region.

Because 2TCM is the compartmental model of choice for ^{18}F-FESCH tracer kinetics, the effect of pretreatment on regional 2TCM V_T was evaluated using 2-way repeated-measures ANOVA. This analysis showed a significant interaction between brain VOI and pretreatment, with Bonferroni posttests demonstrating a significant difference in average V_T between control and pretreated animals for the striatum but not for the hippocampus, midbrain, or cerebellum.

For the pretreated animals, 2TCM DVR − 1 representing striatal ^{18}F-FESCH uptake relative to the hippocampus, midbrain, and cerebellum was, respectively, 1.13 ± 0.20, 1.16 ± 0.43, and 1.09 ± 0.44—that is, not significantly different from 1 (Wilcoxon signed rank test, $P > 0.05$).

^{18}F-FPSCH Versus ^{18}F-FESCH. Using a nonparametric, 2-tailed Mann–Whitney test, no significant differences were found between striatal ^{18}F-FESCH 2TCM V_T (5.0 ± 2.0) and striatal ^{18}F-FPSCH 1TCM V_T (3.7 ± 1.1) in control animals ($P = 0.33$).

^{18}F-FPSCH and ^{18}F-FESCH BP_{ND}

Striatal BP_{ND} was calculated as 1TCM DVR − 1 for ^{18}F-FPSCH and 2TCM DVR − 1 for ^{18}F-FESCH, using the simplified reference tissue model (SRTM) and 90- and 60-min acquisitions. As the reference region, hippocampus, midbrain, and cerebellum were considered.

Control Group. SRTM BP_{ND} data for the control group are presented in Table 3. For this group, 1-way repeated-measures ANOVA (Friedman test) for each tracer and for each candidate reference region revealed no significant differences between striatal BP_{ND} calculated as DVR − 1 and striatal BP_{ND} determined using SRTM and a 90- or 60-min acquisition except for ^{18}F-FPSCH striatal BP_{ND} using midbrain as the reference region. In that case, Dunn multiple-comparison posttesting showed a significant difference between striatal BP_{ND} calculated as 1TCM DVR − 1 and SRTM BP_{ND} determined using a 60-min rather than a 90-min acquisition.

Again, for the control group, a Bland–Altman comparison (% difference) of ^{18}F-FPSCH striatal BP_{ND} calculated as 1TCM DVR − 1 with striatal BP_{ND} for ^{18}F-FPSCH using SRTM and a 90- and 60-min acquisition is presented in Table 4 for the 3 candidate reference regions. This is also presented for ^{18}F-FESCH in Table 5, where striatal BP_{ND} calculated as 2TCM DVR − 1 is compared with SRTM BP_{ND} for a 90- and 60-min acquisition and for the different candidate reference regions. For visual assessment of agreement between the different methods, striatal BP_{ND} calculated as DVR − 1 is also plotted in Figure 3 against SRTM BP_{ND} for a 90- and 60-min acquisition for both tracers and for the different candidate reference regions.

Pretreated Group. For the pretreated group, the BP_{ND} of ^{18}F-FPSCH in the striatum using SRTM and a 90- or 60-min acquisition was, respectively, 0.11 ± 0.07 and 0.12 ± 0.07 (hippocampus as reference), 0.04 ± 0.12 and 0.05 ± 0.11 (midbrain as reference), and 0.04 ± 0.10 and 0.04 ± 0.11 (cerebellum as reference). The corresponding BP_{ND} for ^{18}F-FESCH was 0.16 ± 0.21 and 0.21 ± 0.20, 0.14 ± 0.16 and 0.16 ± 0.15, and 0.04 ± 0.28 and −0.02 ± 0.43, respectively. None of these values significantly differed from 0 (Wilcoxon signed rank test, $P > 0.05$) except for ^{18}F-FPSCH SRTM BP_{ND} for 90- and 60-min acquisitions using hippocampus as the reference region.

^{18}F-FPSCH Versus ^{18}F-FESCH. Comparing striatal BP_{ND} calculated as 1TCM DVR − 1 for ^{18}F-FPSCH with striatal BP_{ND} calculated as 2TCM DVR − 1 for the control group and for each candidate reference region using a nonparametric, 2-tailed Mann–Whitney

TABLE 3
Baseline Striatal BP_{ND} Calculated as DVR − 1 and Using SRTM with 90- and 60-Minute Scans

	^{18}F-FPSCH			^{18}F-FESCH		
Reference region	1TCM (DVR − 1)	SRTM (90 min)	SRTM (60 min)	2TCM (DVR − 1)	SRTM (90 min)	SRTM (60 min)
Hippocampus	2.25 ± 0.35 (15.77%)	2.23 ± 0.27 (12.29%)	2.35 ± 0.22 (9.40%)	2.78 ± 0.70 (25.30%)	2.69 ± 0.68 (25.33%)	2.72 ± 0.64 (23.65%)
Midbrain	2.14 ± 0.41 (19.28%)	2.19 ± 0.41 (18.63%)	2.29 ± 0.33 (14.56%)	2.89 ± 0.34 (11.60%)	2.83 ± 0.38 (13.38%)	2.91 ± 0.33 (11.38%)
Cerebellum	2.19 ± 0.25 (11.64%)	2.28 ± 0.21 (9.09%)	2.33 ± 0.20 (8.83%)	2.91 ± 0.49 (16.94%)	2.78 ± 0.42 (15.24%)	2.80 ± 0.34 (12.28%)

Data are mean ± SD, followed by coefficient of variation in parentheses.

TABLE 4
Bland–Altman Comparison of Striatal BP_{ND} Calculated as 1TCM DVR − 1 and Using SRTM for Baseline ^{18}F-FPSCH PET with 90- and 60-Minute Scans

Parameter	SRTM (90 min)			SRTM (60 min)		
	Hippocampus	Midbrain	Cerebellum	Hippocampus	Midbrain	Cerebellum
Bias (%)	−0.4	2.8	4.4	4.9	7.8	6.9
SD of bias (%)	4.6	5.2	5.8	9.0	6.8	6.4
95% limits of agreement (%)	[−9.4,8.6]	[−7.5,13.0]	[−7.1,15.8]	[−12.8,22.5]	[−5.6,21.2]	[−5.7,19.4]

Data are percentage difference vs. average. Hippocampus, midbrain, and cerebellum were considered as reference region.

test, significant differences were found for the values calculated for the midbrain and cerebellum whereas no significant difference was found for the hippocampus.

DISCUSSION

We evaluated two radiofluorinated analogs of SCH442416, ^{18}F-FPSCH and ^{18}F-FESCH, as ligands for PET imaging of A_{2A} receptor expression in rat brain. On the basis of the Akaike information criterion, 1TCM was the most appropriate model for describing ^{18}F-FPSCH kinetics whereas 2TCM was the most suitable model for ^{18}F-FESCH kinetics. Evaluation of the different compartment models was limited to the tracer kinetics of the subcortical regions, although previous studies with A_{2A} receptor radioligands have used the centrum semiovale (*26,27*) and cerebral cortex as the reference region (*28,29*). However, fitting of 2TCM to tracer uptake in the cortical regions and cerebellum proved problematic for the dynamic ^{18}F-FPSCH scans because of defluorination of the ^{18}F-FPSCH compound, resulting in an accumulation of activity in the skull and other bone structures surrounding the brain, confounding the tracer kinetics of the cortical regions and cerebellum with an irreversible component. For this reason, the standard template-based cerebellar brain volume of interest was adjusted manually to cover only the central part of the cerebellum such that these confounding spillover effects were minimized.

No significant differences were found between the striatal V_T of the two tracers in control animals, although the average V_T in the striatum was higher for ^{18}F-FESCH (2TCM fit) than for ^{18}F-FPSCH (1TCM fit). For both tracers, striatal V_T calculated from a Logan plot was lower than V_T calculated from a compartment model fit, although this difference was significant only for ^{18}F-FPSCH. This observation is in line with literature data reporting that Logan plotting underestimates V_T because of the impact of noise (*29*).

We observed a significant reduction in the striatal V_T of both tracers after pretreatment. On the other hand, no significant pretreatment-induced decrease in V_T occurred in the hippocampus, midbrain, or cerebellum. Moreover, the striatal DVR relative to each of these 3 regions after pretreatment was not significantly different from 1, indicating that nondisplaceable tracer binding in the striatum is identical to that in each of these 3 brain regions. These findings indicate that the hippocampus, midbrain, and cerebellum can be considered suitable candidates for a reference tissue approach to quantifying specific tracer binding in the striatum.

We evaluated SRTM for striatal BP_{ND} calculation in control animals using either hippocampus, midbrain, or cerebellum as the reference region and using 60- and 90-min dynamic PET scans. No significant differences were found between striatal SRTM BP_{ND} and DVR − 1 except for ^{18}F-FPSCH using a 60-min scan and midbrain as the reference region. For the pretreated group, striatal SRTM BP_{ND} for ^{18}F-FPSCH with hippocampus as the reference region differed significantly from 0 although a value of 0 had been expected since full blocking of the A_{2A} receptor was induced by predosing (*23*). Moreover, for ^{18}F-FESCH, striatal SRTM BP_{ND} with hippocampus as the reference region demonstrated a considerably increased coefficient of variation (Table 3) for the control group compared with SRTM BP_{ND} using the other brain regions as the reference region. On the basis of these findings, we conclude that midbrain and cerebellum are the reference regions of choice for SRTM BP_{ND} estimation of ^{18}F-FPSCH and ^{18}F-FESCH uptake in the rat brain. Selecting cerebellum as the reference region for SRTM BP_{ND} quantification of striatal uptake of an A_{2A} receptor–specific PET ligand is also supported by other PET studies (*15,19,20,31*).

TABLE 5
Bland–Altman Comparison of Striatal BP_{ND} Calculated as 2TCM DVR − 1 and Using SRTM for Baseline ^{18}F-FESCH PET with 90- and 60-Minute Scans

Parameter	SRTM (90 min)			SRTM (60 min)		
	Hippocampus	Midbrain	Cerebellum	Hippocampus	Midbrain	Cerebellum
Bias (%)	−3.3	−2.3	−4.4	−1.7	0.6	−3.3
SD of bias (%)	1.7	3.0	3.7	5.0	6.1	8.2
95% limits of agreement (%)	[−6.6,−0.1]	[−8.1,3.5]	[−11.5,2.8]	[−11.4,8.1]	[−11.4,12.6]	[−19.4, 12.7]

Data are percentage difference vs. average. Hippocampus, midbrain, and cerebellum were considered as reference region.

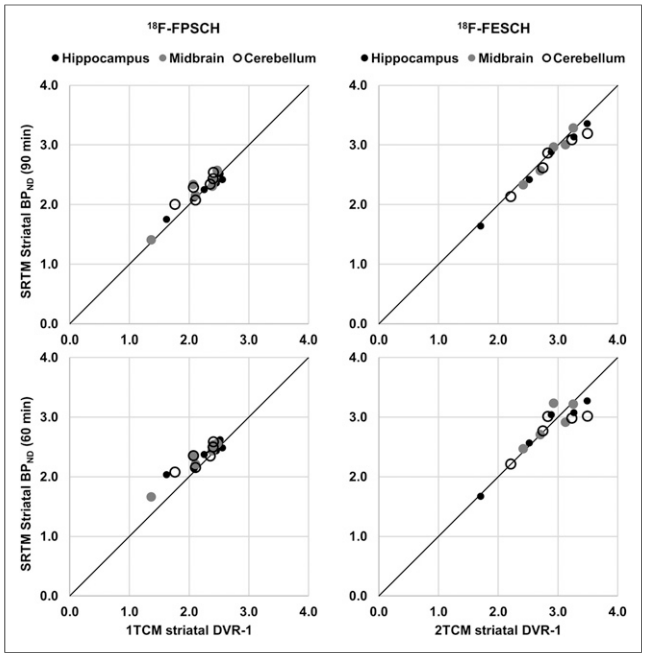

FIGURE 3. Graphical overview of striatal BP_{ND} calculated as DVR − 1 and using SRTM with 90- and 60-min scans.

A Bland–Altman analysis comparing striatal SRTM BP_{ND} with DVR − 1 for ^{18}F-FPSCH (Table 4) and for ^{18}F-FESCH (Table 5) using both 90- and 60-min dynamic PET data demonstrated that both brain regions perform similarly in terms of bias and 95% confidence interval. The scanning time can be reduced to 60 min with a limited increase in bias and 95% confidence interval. For a reduced scanning time of 60 min, cerebellum appeared to perform slightly better as a reference region for ^{18}F-FPSCH quantification, whereas midbrain had the smallest bias and 95% confidence interval for ^{18}F-FESCH quantification. This Bland–Altman analysis also proves that SRTM provides an accurate BP_{ND} for specific striatal ^{18}F-FESCH uptake (Table 5) although 2TCM is the most appropriate compartmental model for tracer ^{18}F-FESCH kinetics in both the striatum and candidate reference regions and SRTM assumes 1TCM tracer kinetics in both reference and target tissue. However, literature data have shown that if the compartmental models of reference and target tissue are matched, the bias induced by SRTM is minimal (*32,33*).

Other A_{2A} receptor–specific PET ligands that have been developed are ^{18}F-MNI-444, ^{11}C-TMSX, ^{11}C-KW-6002, ^{11}C-SCH442416, and ^{11}C-preladenant (*16,23–26,28,30,34*). Except for ^{18}F-MNI-444 and ^{11}C-preladenant, A_{2A} receptor quantification using these tracers is challenging because of the low specific-to-nonspecific binding ratio or high extrastriatal binding. ^{18}F-MNI-444 was tested in rhesus monkeys and humans and demonstrated good brain penetration, with the BP_{ND} ranging from 2.6 to 4.9 in A_{2A} receptor–rich regions (*15,16*). On the other hand, ^{11}C-preladenant has a striatal BP_{ND} of around 5.5 and fast tracer kinetics such that a 60-min acquisition is sufficient for accurate A_{2A} receptor quantification in rat brain. However, ^{11}C-labeled PET tracers have some intrinsic disadvantages due to the short half-life. On the other hand, ^{18}F-FPSCH and ^{18}F-FESCH are fluorinated compounds, therefore providing more flexibility in terms of imaging, and have demonstrated tracer kinetics similar to those of ^{11}C-preladenant, with a BP_{ND} of around 2.5. Comparing ^{18}F-FPSCH and ^{18}F-FESCH, striatal SRTM BP_{ND} using either midbrain or cerebellum as the reference region proved to be significantly lower for ^{18}F-FPSCH than for ^{18}F-FESCH. Taking into account this finding and the Bland–Altman analysis demonstrating the smaller bias for ^{18}F-FESCH than for ^{18}F-FPSCH for a 60-min scan, ^{18}F-FESCH is preferred over ^{18}F-FPSCH for PET imaging of A_{2A} receptor expression in the rat brain. However, for translation into a clinical setting, the presented metabolite results and optimal compartmental models need to be reevaluated for ^{18}F-FESCH brain uptake in humans, because of possible interspecies differences in tracer kinetics and metabolism. Because the cerebellum demonstrated low to negligible A_{2A} receptor density in autoradiography experiments with human brain tissue (*35*), previous studies with A_{2A} receptor–specific radiotracers in humans have used cerebellum as a reference region (*16*). This reference tissue approach could also be considered for the quantification of ^{18}F-FESCH in a clinical setting, thus avoiding the need for arterial sampling and metabolite analysis.

CONCLUSION

We evaluated two radiofluorinated analogs of SCH442416, ^{18}F-FPSCH and ^{18}F-FESCH, as PET ligands for imaging A_{2A} receptor expression in rat brain. Full kinetic analysis using arterial blood sampling indicated 1TCM and 2TCM to be the most suitable models for ^{18}F-FPSCH and ^{18}F-FESCH, respectively. Dynamic PET imaging under baseline and full blocking conditions determined ^{18}F-FESCH to be the most suitable PET ligand for quantifying A_{2A} receptor expression in the rat brain. Accurate quantification of striatum-specific binding is achieved by a 60-min dynamic PET scan and SRTM with either cerebellum or midbrain as the reference region.

DISCLOSURE

No potential conflict of interest relevant to this article was reported.

ACKNOWLEDGMENTS

We thank Jurgen Sijbesma, Mohammed A. Khayum, and Soumen Paul for their technical assistance.

REFERENCES

1. Fredholm BB, Abbracchio MP, Burnstock G, et al. Nomenclature and classification of purinoceptors. *Pharmacol Rev.* 1994;46:143–156.
2. Hess S. Recent advances in adenosine receptor antagonist research. *Expert Opin Ther Pat.* 2001;11:1533–1561.
3. Ishiwata K, Kimura Y, de Vries EFJ, Elsinga PH. PET tracers for mapping adenosine receptors as probes for diagnosis of CNS disorders. *Cent Nerv Syst Agents Med Chem.* 2007;7:57–77.
4. Palmer TM, Stiles GL. Adenosine receptors. *Neuropharmacology.* 1995;34: 683–694.
5. Jacobson KA. Introduction to adenosine receptors as therapeutic targets. *Handb Exp Pharmacol.* 2009;193:1–24.
6. Khanapur S, Paul S, Shah A, et al. Development of [^{18}F]-labeled pyrazolo[4,3-e]-1,2,4-triazolo[1,5-c]pyrimidine (SCH442416) analogs for the imaging of cerebral adenosine A_{2A} receptors with positron emission tomography. *J Med Chem.* 2014;57:6765–6780.
7. Fastbom J, Pazos A, Palacios JM. The distribution of adenosine A1 receptors and 5′-nucleotidase in the brain of some commonly used experimental animals. *Neuroscience.* 1987;22:813–826.
8. Martinez-Mir MI, Probst A, Palacios JM. Adenosine A2 receptors: selective localization in the human basal ganglia and alterations with disease. *Neuroscience.* 1991;42:697–706.

9. Ji XD, Stiles GL, van Galen PJ, Jacobson KA. Characterization of human striatal A2-adenosine receptors using radioligand binding and photoaffinity labeling. *J Recept Res.* 1992;12:149–169.
10. Parkinson FE, Fredholm BB. Autoradiographic evidence for G-protein coupled A2-receptors in rat neostriatum using [^{3}H]-CGS 21680 as a ligand. *Naunyn Schmiedebergs Arch Pharmacol.* 1990;342:85–89.
11. Tavares AA, Batis JC, Papin C, et al. Kinetic modeling, test-retest, and dosimetry of ^{123}I-MNI-420 in humans. *J Nucl Med.* 2013;54:1760–1767.
12. Schiffmann SN, Fisone G, Moresco R, Cunha RA, Ferre S. Adenosine A_2A receptors and basal ganglia physiology. *Prog Neurobiol.* 2007;83:277–292.
13. Schwarzschild MA, Agnati L, Fuxe K, Chen JF, Morelli M. Targeting adenosine A_{2A} receptors in Parkinson's disease. *Trends Neurosci.* 2006;29:647–654.
14. Ferré S, Quiroz C, Orru M, et al. Adenosine A_{2A} receptors and A_{2A} receptor heteromers as key players in striatal function. *Front Neuroanat.* 2011;5:36.
15. Barret O, Hannestad J, Alagille D, et al. Adenosine 2A receptor occupancy by tozadenant and preladenant in rhesus monkeys. *J Nucl Med.* 2014;55:1712–1718.
16. Barret O, Hannestad J, Vala C, et al. Characterization in humans of ^{18}F-MNI-444, a PET radiotracer for brain adenosine 2A receptors. *J Nucl Med.* 2015;56:586–591.
17. Bhattacharjee AK, Lang L, Jacobson O, et al. Striatal adenosine A_{2A} receptor mediated PET imaging in 6-hydroxydopamine lesioned rats using [^{18}F]-MRS5425. *Nucl Med Biol.* 2011;38:897–906.
18. Hirani E, Gillies J, Karasawa A, et al. Evaluation of [4-O-methyl-^{11}C]KW-6002 as a potential PET ligand for mapping central adenosine A_{2A} receptors in rats. *Synapse.* 2001;42:164–176.
19. Ishiwata K, Noguchi J, Wakabayashi S, et al. ^{11}C-labeled KF18446: a potential central nervous system adenosine A_{2a} receptor ligand. *J Nucl Med.* 2000;41:345–354.
20. Moresco RM, Todde S, Belloli S, et al. In vivo imaging of adenosine A_{2A} receptors in rat and primate brain using [^{11}C]SCH442416. *Eur J Nucl Med Mol Imaging.* 2005;32:405–413.
21. Noguchi J, Ishiwata K, Wakabayashi S, et al. Evaluation of carbon-11-labeled KF17837: a potential CNS adenosine A_{2a} receptor ligand. *J Nucl Med.* 1998;39:498–503.
22. Stone-Elander S, Thorell JO, Eriksson L, Fredholm BB, Ingvar M. In vivo biodistribution of [N-^{11}C-methyl]KF 17837 using 3-D-PET: evaluation as a ligand for the study of adenosine A_{2A} receptors. *Nucl Med Biol.* 1997;24:187–191.
23. Zhou X, Khanapur S, de Jong JR, et al. In vivo evaluation of [^{11}C]preladenant positron emission tomography for quantification of adenosine A_{2A} receptors in the rat brain. *J Cereb Blood Flow Metab.* February 25, 2016.
24. Julien-Dolbec C, Tropres I, Montigon O, et al. Regional response of cerebral blood volume to graded hypoxic hypoxia in rat brain. *Br J Anaesth.* 2002;89: 287–293.
25. Brooks DJ, Doder M, Osman S, et al. Positron emission tomography analysis of [^{11}C]KW-6002 binding to human and rat adenosine A_{2A} receptors in the brain. *Synapse.* 2008;62:671–681.
26. Naganawa M, Kimura Y, Mishina M, et al. Quantification of adenosine A_{2A} receptors in the human brain using [^{11}C]TMSX and positron emission tomography. *Eur J Nucl Med Mol Imaging.* 2007;34:679–687.
27. Mishina M, Ishiwata K, Kimura Y, et al. Evaluation of distribution of adenosine A_{2A} receptors in normal human brain measured with [^{11}C]TMSX PET. *Synapse.* 2007;61:778–784.
28. Mishina M, Kimura Y, Naganawa M, et al. Differential effects of age on human striatal adenosine A_1 and A_{2A} receptors. *Synapse.* 2012;66:832–839.
29. Mishina M, Ishiwata K, Naganawa M, et al. Adenosine A_{2A} receptors measured with [C]TMSX PET in the striata of Parkinson's disease patients. *PLoS One.* 2011;6:e17338.
30. Slifstein M, Laruelle M. Effects of statistical noise on graphic analysis of PET neuroreceptor studies. *J Nucl Med.* 2000;41:2083–2088.
31. Ramlackhansingh AF, Bose SK, Ahmed I, Turkheimer FE, Pavese N, Brooks DJ. Adenosine 2A receptor availability in dyskinetic and nondyskinetic patients with Parkinson disease. *Neurology.* 2011;76:1811–1816.
32. Slifstein M, Parsey RV, Laruelle M. Derivation of [^{11}C]WAY-100635 binding parameters with reference tissue models: effect of violations of model assumptions. *Nucl Med Biol.* 2000;27:487–492.
33. Salinas CA, Searle GE, Gunn RN. The simplified reference tissue model: model assumption violations and their impact on binding potential. *J Cereb Blood Flow Metab.* 2015;35:304–311.
34. Naganawa M, Mishina M, Sakata M, et al. Test-retest variability of adenosine A_{2A} binding in the human brain with ^{11}C-TMSX and PET. *EJNMMI Res.* 2014;4:76.
35. Svenningsson P, Hall H, Sedvall G, Fredholm BB. Distribution of adenosine receptors in the postmortem human brain: an extended autoradiographic study. *Synapse.* 1997;27:322–335.